IOP Publishing Nanotechnology
Nanotechnology **26** (2015) 025502 (9pp) doi:10.1088/0957-4484/26/2/025502

Fluctuations due to association and dissociation processes at nanowire-biosensor surfaces and their optimal design

Gerhard Tulzer[1] **and Clemens Heitzinger**[1,2]

[1] Vienna University of Technology, Wiedner Hauptstrasse 8-10, A-1040 Vienna, Austria
[2] School of Mathematical and Statistical Sciences, Arizona State University, Tempe, AZ 85287, USA

E-mail: gerhard.tulzer@tuwien.ac.at and clemens.heitzinger@asu.edu

Received 5 August 2014, revised 19 September 2014
Accepted for publication 2 October 2014
Published 17 December 2014

Abstract

In this work, we calculate the effect of the binding and unbinding of molecules at the surface of a nanowire biosensor on the signal-to-noise ratio of the sensor. We model the fluctuations induced by association and dissociation of target molecules by a stochastic differential equation and extend this approach to a coupled diffusion-reaction system. Where possible, analytic solutions for the signal-to-noise ratio are given. Stochastic simulations are performed wherever closed forms of the solutions cannot be derived. Starting from parameters obtained from experimental data, we simulate DNA hybridization at the sensor surface for different target molecule concentrations in order to optimize the sensor design.

Keywords: fluctuations, nanowire biosensors, simulation

(Some figures may appear in colour only in the online journal)

1. Introduction

Nanowire field-effect sensors have been demonstrated experimentally for the detection of several types of biomolecules in liquids [1–6]. They provide fast, efficient, and label-free detection. In previous works, we have developed mathematical models for the average sensor response including the screening of the biomolecules by free ions in the liquid and we have quantified these effects in simulation studies of nanowire biosensors [7–12] as well as nanowire gas sensors [13].

In this work, we model and simulate fluctuations and noise due to binding and unbinding events at the surface of a nanowire biosensor. Since the random nature of DNA hybridization, i.e., random motion and random interaction, causes so-called *biological noise* [14–18], we consider these reactions as stochastic processes allowing quantification of the noise induced during detection. Moreover, we take into account that the number of target molecules in the liquid is limited and therefore couple the equations of DNA hybridization with a diffusion equation in the liquid phase.

When investigating the coupled system, there are in principle three regimes to consider.

- Probe-target binding is much faster than diffusion: here, one should consider deterministic equations for the chemical reactions coupled with a stochastic diffusion equation. The effect of the coupling only enters through a boundary condition for the diffusion equation.
- Diffusion is much faster than probe-target binding: this is the opposite case, where the sensor is limited by diffusion.
- Both processes occur at comparable speeds: now the whole system must be considered in a coupled stochastic formulation. A parameter estimation for the chemical reactions shows that this is indeed the case in the nanowire sensors of interest (see section 4.1 below). We will focus on this case throughout this study.

To obtain quantitative results, we rely on experimental data from [19], where the effect of probe density at the nanowire surface was investigated. We estimate reaction parameters from those results and use them for stochastic simulations.

The paper is organized as follows: in section 2, the deterministic reaction model without diffusion is described and extended to a stochastic version. Expected value, variance, and signal-to-noise ratio (SNR) are given in explicit form. In section 3, we couple the system to a diffusion equation and describe the algorithm used in the simulation. We present numerical results in section 4 and discuss them in section 5.

2. The binding model

We consider the surface of a nanowire sensor which is functionalized with probe molecules and surrounded by an aqueous solution containing the target molecules. Probe-target binding, or DNA hybridization in particular, is then described by association and dissociation processes taking place at the sensor surface. The reactions considered are

$$\mathbf{T} + \mathbf{P} \xrightarrow{r_\mathrm{a}} \mathbf{PT}, \tag{1a}$$

$$\mathbf{PT} \xrightarrow{r_\mathrm{d}} \mathbf{T} + \mathbf{P}, \tag{1b}$$

where **T** denotes a target molecule, **P** denotes a probe molecule and **PT** denotes a probe-target complex at the sensor surface and r_a and r_d are reaction constants, namely the association and the dissociation constants.

2.1. A deterministic approach

To gain first insights into the system, we consider large enough amounts of target as well as probe molecules such that random effects are negligible. With these approximations, the reactions then correspond to an ordinary differential equation (ODE) by application of the mass action law, yielding

$$\frac{\mathrm{d}\mathbf{PT}}{\mathrm{d}t}(t) = r_\mathrm{a} C_\mathrm{T}\big(C_\mathrm{P} - \mathbf{PT}(t)\big) - r_\mathrm{d}\mathbf{PT}(t), \tag{2a}$$

$$\mathbf{PT}(0) = 0, \tag{2b}$$

where C_T and C_P are the concentrations of target molecules in the liquid near the surface and probe molecules at the surface, respectively. The initial condition indicates that there are no probe-target complexes present at the surface in the beginning. From this equation, the concentration of **PT** complexes at the surface can be computed for any time.

Under the (simplifying) assumption of constant target-molecule concentration, this ODE can be solved in a straightforward manner, yielding

$$\begin{aligned}\mathbf{PT}(t) &= \frac{r_\mathrm{a} C_\mathrm{P} C_\mathrm{T}}{r_\mathrm{a} C_\mathrm{T} + r_\mathrm{d}} \cdot \left(1 - \mathrm{e}^{-(r_\mathrm{a} C_\mathrm{T} + r_\mathrm{d})t}\right) \\ &= \frac{\alpha}{\beta} \cdot \left(1 - \mathrm{e}^{-\beta t}\right),\end{aligned} \tag{3}$$

where we used the abbreviations

$$\alpha := r_\mathrm{a} C_\mathrm{P} C_\mathrm{T}, \tag{4}$$

$$\beta := r_\mathrm{a} C_\mathrm{T} + r_\mathrm{d}. \tag{5}$$

If, however, the concentrations of the target molecules vary, the situation is not as simple and will be considered below.

2.2. Stochastic formulation

The deterministic approach discussed in the previous section is a convenient method in case there is a sufficiently large number of molecules taking part in the association–dissociation or hybridization processes. However, since we are interested in detection limits, it is essential to consider cases when only a few molecules are present in the system. This requires a more detailed approach taking into account that the association and dissociation processes occur in a stochastic manner. Therefore, we model both reactions at the surface as stochastic processes. This approach yields a chemical Langevin equation [20].

The number **PT** of probe-target complexes now becomes a random variable and we will write X_t for this quantity in the following. Denoting the number of associations (respectively dissociations) within a time interval τ by the random variable $\mathcal{P}_a(X_t, \tau)$ (respectively $\mathcal{P}_d(X_t, \tau)$), we can write a difference equation for X_t as

$$X_{t+\tau} - X_t = \mathcal{P}_a\big(X_t, \tau\big) - \mathcal{P}_d\big(X_t, \tau\big). \tag{6}$$

The number of reactions taking place is a counting process. Therefore, both random variables obey a Poisson distribution with parameters

$$a\big(X_t, \tau\big) = \tau r_\mathrm{a} C_\mathrm{T}\big(C_\mathrm{P} - X_t\big), \tag{7}$$

$$d\big(X_t, \tau\big) = \tau r_\mathrm{d} X_t. \tag{8}$$

Here $a(X_t, \tau)$ is the parameter of the Poisson process $\mathcal{P}_a$ describing association and $d(X_t, \tau)$ is the parameter of $\mathcal{P}_d$ describing dissociation. $a(X_t, \tau)$ is proportional to the time interval τ, to the association rate r_a, to the number C_T of target molecules available for binding, and to the number $C_P - X_t$ of available binding sites; $d(X_t, \tau)$ is proportional to the time interval τ, to the dissociation rate r_d, and to the number X_t of bound target molecules. This is analog to (2a) above.

If we consider the time interval τ to be large enough so that many reactions occur within it [21], we can approximate the Poisson distributed random variables by normal distributed random variables with the same mean and variance. Therefore, we find

$$\mathcal{P}_a\big(X_t, \tau\big) = a\big(X_t, \tau\big) + \sqrt{a\big(X_t, \tau\big)}\,\mathcal{N}(0, 1), \tag{9}$$

$$\mathcal{P}_d\big(X_t, \tau\big) = d\big(X_t, \tau\big) + \sqrt{d\big(X_t, \tau\big)}\,\mathcal{N}(0, 1). \tag{10}$$

Hence, equation (6) becomes a Langevin equation in white-noise form

$$\begin{aligned}\mathrm{d}X_t &= \big(r_\mathrm{a} C_\mathrm{T}\big(C_\mathrm{P} - X_t\big) - r_\mathrm{d} X_t\big)\mathrm{d}t \\ &\quad + \sqrt{r_\mathrm{a} C_\mathrm{T}\big(C_\mathrm{P} - X_t\big)}\,\mathrm{d}B_1 - \sqrt{r_\mathrm{d} X_t}\,\mathrm{d}B_2 : \\ X_0 &= 0,\end{aligned} \tag{11}$$

where $\mathrm{d}B_1$ and $\mathrm{d}B_2$ are two independent Wiener processes. We are interested in the statistics of the random variable X_t and therefore we calculate the first and the second moment.

Again, the situation is much more complicated if the target concentration is not constant. For example, it is only possible to obtain explicit expressions under the assumption of constant target concentration, which is assumed to hold in the rest of this section. Varying target concentrations will be considered in section 3.

2.3. Calculation of the first moment

To calculate the first moment, we simply apply the expectancy to equation (11) to find

$$\begin{aligned}\mathrm{d}\mathbb{E}\left(X_t\right) &= r_\mathrm{a} C_\mathrm{T}\left(C_\mathrm{P} - \mathbb{E}\left(X_t\right)\right)\mathrm{d}t - r_\mathrm{d}\mathbb{E}\left(X_t\right)\mathrm{d}t \\ &\quad + \underbrace{\mathbb{E}\left(\sqrt{r_\mathrm{a} C_\mathrm{T}\left(C_\mathrm{P} - X_t\right)}\,\mathrm{d}B_1\right)}_{=0} \\ &\quad - \underbrace{\mathbb{E}\left(\sqrt{r_\mathrm{d} X_t}\,\mathrm{d}B_2\right)}_{=0} \end{aligned} \tag{12}$$

simplifying to

$$\frac{\mathrm{d}\mathbb{E}\left(X_t\right)}{\mathrm{d}t} = r_\mathrm{a} C_\mathrm{T}\left(C_\mathrm{P} - \mathbb{E}\left(X_t\right)\right) - r_\mathrm{d}\mathbb{E}\left(X_t\right). \tag{13}$$

This is the same equation as (2a), but now for $\mathbb{E}(X_t)$, and hence the solution is

$$E(t) := \mathbb{E}\left(X_t\right) = \frac{\alpha}{\beta}\left(1 - \mathrm{e}^{-\beta t}\right) \tag{14}$$

for the initial condition $\mathbb{E}(X_t) = 0$. This justifies the use of the deterministic equation for the parameter estimation in section 4.1.

2.4. Calculation of the second moment

The calculation of the second moment is more involved. First, we define the random variable $Y_t := X_t^2$. Applying Itō's formula to Y_t gives

$$\mathrm{d}Y_t = 2X_t\,\mathrm{d}X_t + \mathrm{d}X_t\,\mathrm{d}X_t. \tag{15}$$

Substituting for $\mathrm{d}X_t$ and using $\mathrm{d}B_i\,\mathrm{d}B_j = \delta_{ij}\mathrm{d}t$ as well as $\mathrm{d}t\,\mathrm{d}t = 0$ and $\mathrm{d}t\,\mathrm{d}B_i = 0$, we obtain

$$\begin{aligned}\mathrm{d}\left(X_t^2\right) &= \left(r_\mathrm{a} C_\mathrm{T} C_\mathrm{P} + \left(2r_\mathrm{a} C_\mathrm{T} C_\mathrm{P} - r_\mathrm{a} C_\mathrm{T} + r_\mathrm{d}\right)X_t\right)\mathrm{d}t \\ &\quad - 2\left(r_\mathrm{a} C_\mathrm{T} + r_\mathrm{d}\right)X_t^2\,\mathrm{d}t \\ &\quad + 2X_t\left(\sqrt{r_\mathrm{a} C_\mathrm{T}\left(C_\mathrm{P} - X_t\right)}\,\mathrm{d}B_1 - \sqrt{r_\mathrm{d} X_t}\,\mathrm{d}B_2\right). \end{aligned} \tag{16}$$

Applying the expectancy, we obtain

$$\begin{aligned}\mathrm{d}\mathbb{E}\left(X_t^2\right) &= \alpha\mathrm{d}t + \left(2\alpha - r_\mathrm{a} C_\mathrm{T} + r_\mathrm{d}\right)\mathbb{E}\left(X_t\right)\mathrm{d}t - 2\beta\mathbb{E}\left(X_t^2\right)\mathrm{d}t \\ &\quad + \left(\underbrace{\mathbb{E}\left(2X_t\sqrt{r_\mathrm{a} C_\mathrm{T}\left(C_\mathrm{P} - X_t\right)}\,\mathrm{d}B_1\right)}_{=0}\right. \\ &\quad \left. - \underbrace{\mathbb{E}\left(2X_t\sqrt{r_\mathrm{d} X_t}\,\mathrm{d}B_2\right)}_{=0}\right) \end{aligned} \tag{17}$$

and furthermore

$$\begin{aligned}\frac{\mathrm{d}\mathbb{E}\left(X_t^2\right)}{\mathrm{d}t} &= \alpha + \left(2\alpha - r_\mathrm{a} C_\mathrm{T} + r_\mathrm{d}\right)\frac{\alpha}{\beta}\left(1 - \mathrm{e}^{-\beta t}\right) \\ &\quad - 2\beta\mathbb{E}\left(X_t^2\right). \end{aligned} \tag{18}$$

The solution of this equation with the initial condition $\mathbb{E}(X_t^2) = 0$ is given by

$$\begin{aligned}P(t) &:= \mathbb{E}\left(X_t^2\right) \\ &= \frac{\alpha}{\beta^2}\left(\alpha + r_\mathrm{d} + \left(r_\mathrm{a} C_\mathrm{T} - 2\alpha - r_\mathrm{d}\right)\mathrm{e}^{-\beta t}\right. \\ &\quad \left. + \left(\alpha - r_\mathrm{a} C_\mathrm{T}\right)\mathrm{e}^{-2\beta t}\right). \end{aligned} \tag{19}$$

Therefore, the variance of X_t is given by

$$\begin{aligned}\mathbb{V}\left(X_t\right) &= \mathbb{E}\left(X_t^2\right) - \mathbb{E}\left(X_t\right)^2 = P(t) - E(t)^2 \\ &= \frac{\alpha}{\beta^2}\left(r_\mathrm{d} + \left(r_\mathrm{a} C_\mathrm{T} - r_\mathrm{d}\right)\mathrm{e}^{-\beta t} - r_\mathrm{a} C_\mathrm{T}\mathrm{e}^{-2\beta t}\right) \\ &= \frac{\alpha}{\beta^2}\left(1 - \mathrm{e}^{-\beta t}\right)\left(r_\mathrm{d} + r_\mathrm{a} C_\mathrm{T}\mathrm{e}^{-\beta t}\right). \end{aligned} \tag{20}$$

An alternative derivation starts from the binding probability

$$p(t) := \frac{E(t)}{C_\mathrm{P}} = \frac{\alpha}{C_\mathrm{P}\beta}\left(1 - \mathrm{e}^{-\beta t}\right),$$

so that we find

$$\mathbb{V}\left(X_t\right) = C_\mathrm{P} p(t)(1 - p(t)) = \frac{\alpha}{\beta^2}\left(1 - \mathrm{e}^{-\beta t}\right)\left(r_\mathrm{d} + r_\mathrm{a} C_\mathrm{T}\mathrm{e}^{-\beta t}\right)$$

for the variance $\mathbb{V}(X_t)$ after a calculation assuming binomial statistics. This is the same as (20).

2.5. The SNR

One of the most important characteristics of a sensor is its signal-to-noise ratio (SNR). This quantity measures the quality of a signal and also determines the threshold of distinguishing it from background noise data. While the signal is related to the expected value, the noise is related to the

variance. Hence the SNR is defined as the ratio

$$\mathrm{SNR}(t) := \frac{\mathbb{E}(X_t)}{\sqrt{\mathbb{V}(X_t)}} \tag{21}$$

of expected value and standard deviation of the random variable. This ratio is a dimensionless value. Using the above calculations, we find

$$\begin{aligned}\mathrm{SNR}(t) &:= \frac{\mathbb{E}(X_t)}{\sqrt{\mathbb{V}(X_t)}} \\ &= \sqrt{\alpha}\,\frac{1-\mathrm{e}^{-\beta t}}{\sqrt{\left(1-\mathrm{e}^{-\beta t}\right)\left(r_\mathrm{d}+r_\mathrm{a}C_\mathrm{T}\mathrm{e}^{-\beta t}\right)}}.\end{aligned} \tag{22}$$

Note that the SNR has a finite value as $t \to \infty$ namely

$$\lim_{t\to\infty}\mathrm{SNR}(t) = \sqrt{\frac{C_\mathrm{P}C_\mathrm{T}r_\mathrm{a}}{r_\mathrm{d}}}, \tag{23}$$

which is easily interpreted when the SNR is to be maximized.

3. The coupled model

When modeling realistic sensors, it is not sufficient to think of the target molecules near the surface as a reservoir, i.e., having a constant concentration. The diffusion of the target molecules in the aqueous solution surrounding the sensor must be included. Diffusion will slow down the binding of target molecules at the sensor surface, because after an initial phase the target molecules deplete near the surface and their diffusion to the sensor surface requires time. (This effect will be observed numerically in section 4.)

From the modeling point of view, the coefficient $C_\mathrm{T} = C_\mathrm{T}(t)$ is now a time-dependent function and can be obtained from the solution of the diffusion equation

$$\frac{\partial u}{\partial t} = D\Delta u \quad \text{in } \Omega\times(0,T], \tag{24a}$$

$$\nu\cdot\nabla u = g \quad \text{on } \partial\Omega\times(0,T] \tag{24b}$$

$$u(x,0) = u_0 \qquad \text{in } \Omega. \tag{24c}$$

In fact, $C_\mathrm{T}(t)$ is the mean value of u near the surface. Here, $u(x, t)$ is the concentration of the target molecules. The function g at the Neumann boundary represents the fact that the number of molecules decreases at the surface according to the association–dissociation process, while at the rest of the boundary, there is no flow.

The parameter D is the diffusion constant of the target molecules. In the case of single-stranded DNA oligomers, which are modeled as rods, its numerical value is obtained via

$$D = \frac{Ak_BT}{3\pi\eta L_\mathrm{DNA}} = 8.8775\times10^{-11}\,\mathrm{m^2\,s^{-1}}, \tag{25}$$

where η is the liquid viscosity, which is determined depending on salt concentration and temperature, L_DNA is the length of the DNA oligomers, and A is a correction factor according to [22]. The numerical values of these parameters are given in table 1.

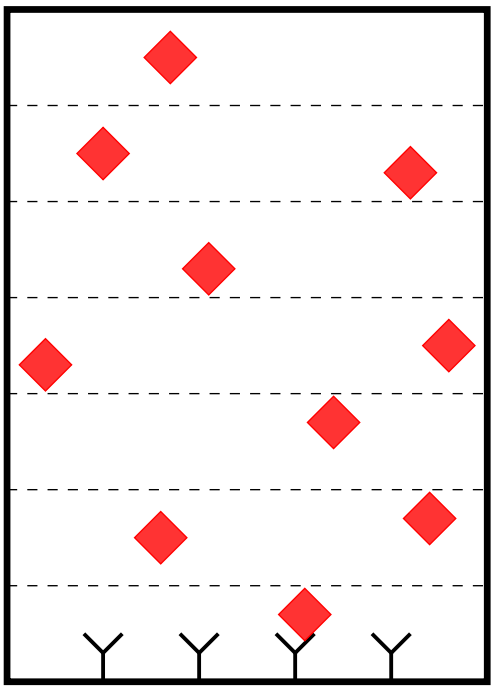

Figure 1. Sketch of the domain. The Y-shaped objects are the probe molecules and the red diamonds represent the target molecules. The whole domain is partioned in several boxes according to the simulation algorithm described in section 3.1.

Another approach to model the diffusion constant of single-stranded DNA oligomers is to use the persistence length. In [23, page F] it is assumed to be between 0.6 nm and 1.3 nm depending on the ionic strength of the solution. Using these values, the diffusion constant is between $3.45\times10^{-10}\,\mathrm{m^2\,s^{-1}}$ and $1.72\times10^{-10}\,\mathrm{m^2\,s^{-1}}$, respectively. Since the persistence length of ssDNA oligomers is still controversial [23], the value of D in (25) is used in the following.

The simulations below can be performed for any number of spatial dimensions in (24a)–(24c). Because of the usual geometry of the analyte compartment above a nanowire transducer, it suffices to consider the one-dimensional case, where the axis is perpendicular to the sensor surface, in order to capture the dynamics of particles diffusing towards the sensor surface, and this is the case investigated in the following (see also figure 1). Extensions to higher dimensions are straightforward.

This initial-value problem has to be coupled with the association–dissociation process modeled in section 2. The quantity that enters the stochastic differential equation is the target-molecule concentration in the surface region, which can generally not be obtained in explicit form. Therefore, the solution of stochastic differential equation for the association–dissociation process can generally not be obtained in explicit form as well, and hence numerical investigations are necessary.

Table 1. Parameters used for the computation of the diffusion constant.

Parameter	Numerical value	Comment	Reference
A	2.074	correction factor	[22]
k_B	$1.380\,65 \times 10^{-23}$ J K^{-1}	Boltzmann constant	—
T	298.15 K	temperature in Kelvin	[19]
η	9.719×10^{-4} N s m^{-2}	viscosity	[24]
L_{DNA}	10.5 nm	length of molecules	[19]

As will turn out after the estimation of the association and dissociation constants, the speed of diffusion is of comparable size, and therefore we also have to consider a stochastic version of the diffusion equation.

3.1. Stochastic simulation

The numerical simulation of the stochastic reaction-diffusion processes investigated here is performed according to the algorithm described in [25]. The problem can be reduced to only one spatial dimension. We divide the domain of the aqueous solution into a certain number of boxes, where diffusion is represented as the transition of molecules between two adjacent compartments. A sketch of the domain is shown in figure 1. Target binding is modeled by adding another (virtual) box, where only transitions to and from the compartment representing the surface layer can occur.

The algorithm consists of the following steps:

(i) Choose the time interval τ randomly according to the reaction constants, the diffusion constant, and the number of particles in the respective compartments.
(ii) Choose the two involved boxes for the transition occurring during the time interval τ as random numbers.
(iii) Update the number of particles in the respective boxes.
(iv) Unless the total simulation time is reached, go to step 1.

For the surface boxes, the transition probabilites are proportional to the reaction rates of the association-diffusion process and to the number of particles, whereas for the rest of the boxes, the transition probability is proportional to the diffusion constant and the number of particles.

To obtain the statistics for the probe-target complexes, the algorithm must be repeated many times in order to calculate the mean value and the variance and hence the SNR at each time. This procedure allows easy parallelization during computation, since every run is independent of the others.

4. Numerical results

In this section, simulation results of realistic field-effect sensors are presented. We consider DNA sensors, because they are important in applications and have been studied well experimentally. Of course, the models from the previous sections can be applied to any pairs of probe and target molecules.

4.1. Determining the reaction rates for DNA hybridization

To perform simulations of nanowire sensors according to the models discussed in the previous sections, it is necessary to find numerical values for the parameters r_a and r_d first. These can be obtained using a least-squares optimization with respect to experimental measurements. We used data reported in [19], where the hybridization kinetics of ssDNA under different probe densities was investigated. By comparing the calculated solutions for the deterministic reaction kinetics to the data, we determined the parameters of interest, which will then be used for simulations throughout this study. The numerical values are shown in table 2. A graphical representation is given in figure 2. The agreement between the experimental data and the calculated curves is shown in figure 3.

The numerical values of the association rate r_a clearly reflect the decrease of the association rates with increased probe density, which is due to to electrostatic repulsion. Analogously, the dissociation rates r_d are hardly affected by the probe density.

4.2. SNR in the case of constant target concentration

Having determined the reaction rates, we can compute the SNR in the case of constant target concentration according to equation (22). The results are shown in figure 4.

It turns out—quite surprisingly—that the SNR is higher when the probe-molecule density is lower. However, this fact is also represented by the formula given in (23).

4.3. SNR in the coupled model

In order to study the effect of diffusion on the target-molecule concentration, we calculate the statistics for the whole system with the same parameters as used in the previous section. The concentrations of probe-target complexes at the surface calculated by the pure reaction model and by the diffusion-reaction system differ as shown in figure 5. This motivates further investigations of the coupled diffusion-reaction system below.

4.4. Different target concentrations and optimal sensor surface design

To optimize sensor design, we now investigate the optimal probe-molecule density for a given target molecule concentration. This knowledge is important to determine the detection limit and to design the most effective sensor for the

Table 2. Reaction parameters for DNA hybridization. The very left column gives the different probe densities.

molecules cm^{-2}	association rate r_a	dissociation rate r_d
2×10^{12}	3933	0.0016
3×10^{12}	4071	0.0042
5.2×10^{12}	1014	0.0019
9.5×10^{12}	861	0.0037
12×10^{12}	348	0.0027

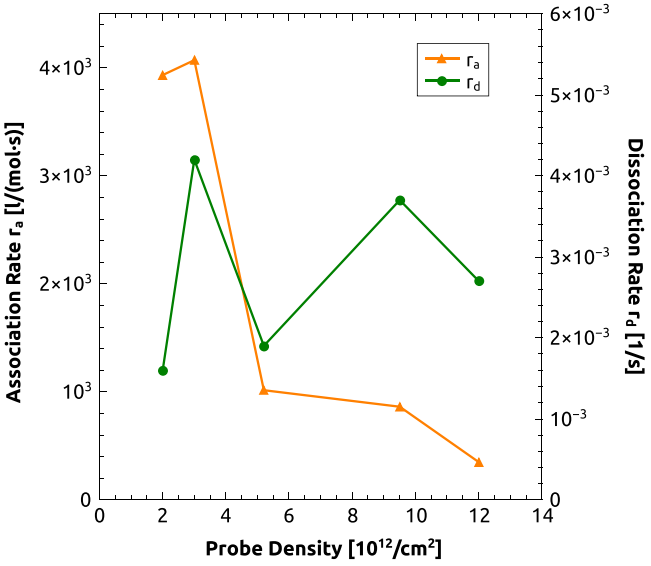

Figure 2. Reaction parameters versus probe-molecule density. For higher probe densities, the association rate decreases significantly.

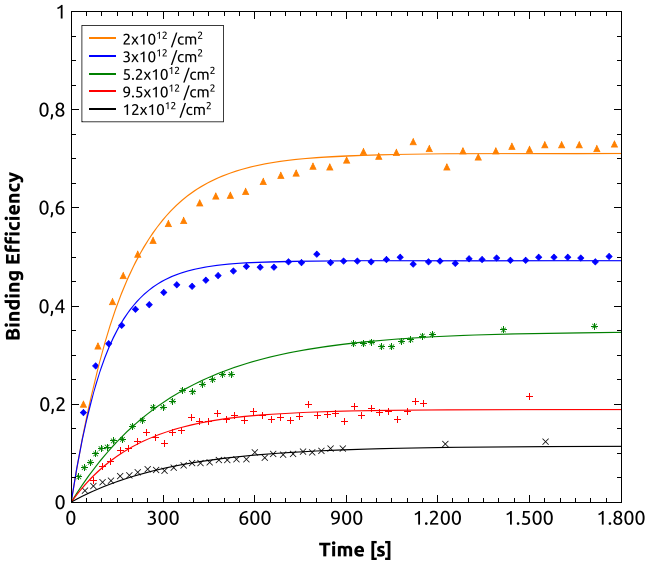

Figure 3. Experimental data from [19] (points) and simulated curves with the calculated parameters (lines). The parameters reflect the decreasing binding efficiency with increasing probe density.

target-molecule concentration regime of interest. To this end, a set of simulations with different parameter values was carried out. The concentrations of used target-molecules range from 1 nM to 270 μM.

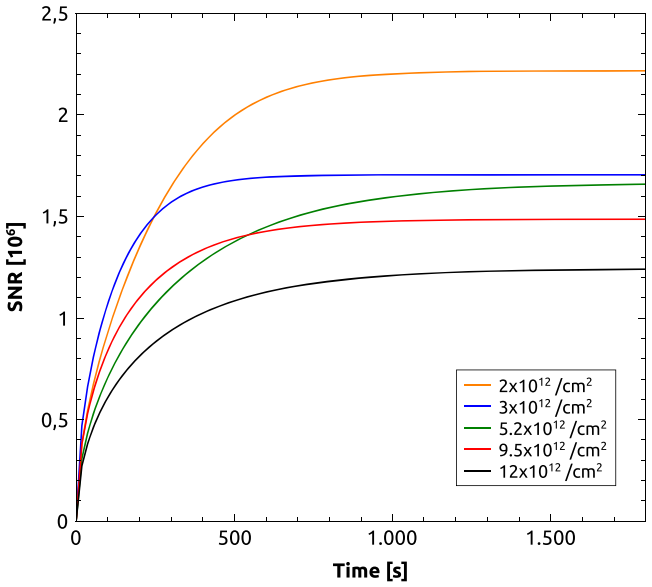

Figure 4. SNR for different probe-molecule concentrations.

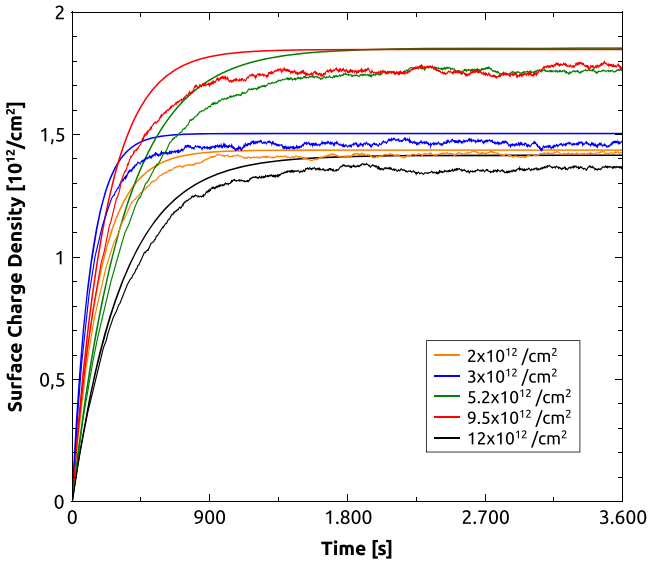

Figure 5. Comparison of solutions of the reaction model and the reaction-diffusion system. The differences are significant.

There are two different quantities of interest when analyzing the results. On the one hand, the binding efficiency is the ratio of hybridized complexes at the surface to the total number of probe molecules. On the other hand, the surface-charge density is proportional to the total number of hybridized complexes per surface area.

The necessity of considering the surface-charge density over binding efficiency becomes clear when investigating very low target and probe concentrations: in this case, the binding efficiency may be large, but the hybridized complexes barely influence the sensor signal since the surface-charge density is barely changed so that the absolute signal is small. On the other hand, since the relative change in binding efficiency may be considerable, it leads to a considerable

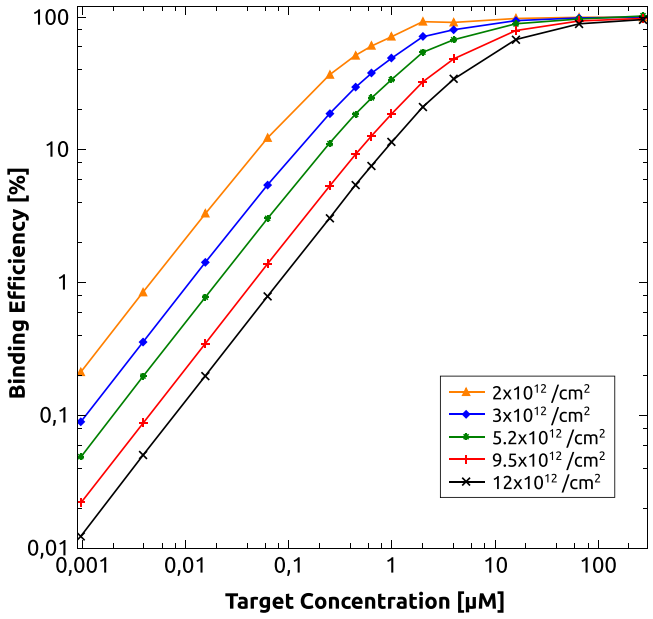

Figure 6. Binding efficiency as a function of target-molecule concentration. The different curves represent different probe densities at the surface (numerical values indicated in the legend). At sufficiently high concentrations, all the probe molecules are hybridized.

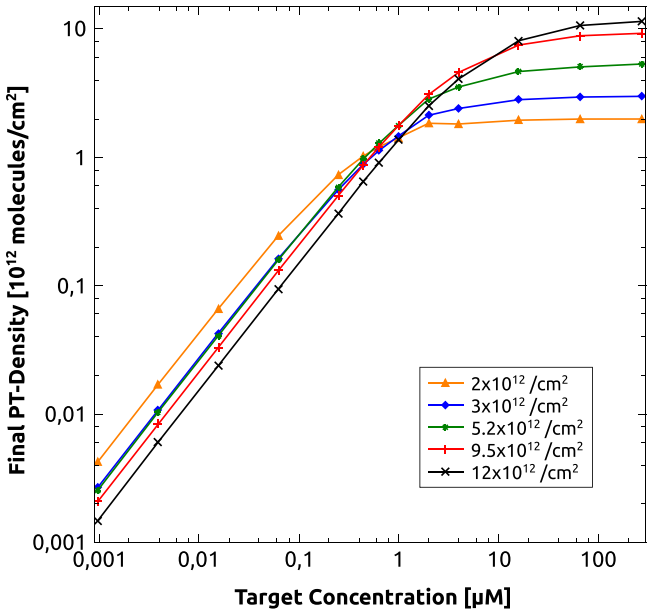

Figure 7. Equilibrium **PT** density depending on target-molecule concentration. Inversion of the optimal probe density occurs around 1 μM.

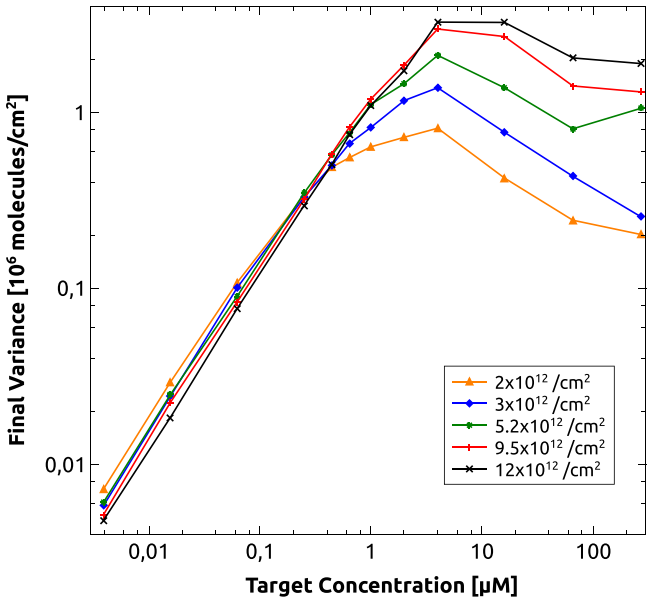

Figure 8. Standard deviation of the number of **PT** complexes at the surface with respect to the target concentration. At high concentrations, the value decreases since almost all probe molecules are hybridized.

change in the sensor signal, so that detection may be possible even if the binding efficiency is very low.

As can be seen in figure 6, the binding efficiency attains a perfect value of (nearly) 100% when the target molecule concentration is large enough. The threshold value for this situation becomes larger with increasing probe density. For low target-molecule concentrations, the binding efficiencies differ by constant values for a given target-molecule concentration.

The situation is quite different when considering the surface-charge density. The simulation results are shown in figure 7. For low target concentrations, lower probe densities yield higher surface-charge densities, while for higher target-molecule concentrations, it is the other way round. The inversion of the optimal probe density happens at around 1 μM target-molecule concentration. This is an important observation, since it means that the probe density is an important design parameter that must be adjusted to the target-molecule concentrations of interest in order to get optimal sensor responses.

Considering the equilibrium state at the surface, one can see in figure 8 that the variance decreases with increasing target-molecule concentration above a certain threshold value. Since the signal is also higher at higher concentrations, target concentration in this region are advantageous; the corresponding SNR is shown in figure 9.

In these numerical simulations, the case of DNA probes and DNA target molecules has been investigated in depth, since this type of sensor is of great practical significance. Of course, the actual numerical results will be different for other combinations of probe and target molecules, e.g., for PNA probes and DNA targets or antibody probes and antigen targets, depending on their charges and association and dissociation constants.

4.5. Different initial conditions

Finally: we investigate how mixing of the aqueous solution affects sensor performance. This question was investigated experimentally in [3]. We consider two different initial conditions here. In the first case, the liquid has been mixed perfectly and the initial concentration of the target molecules

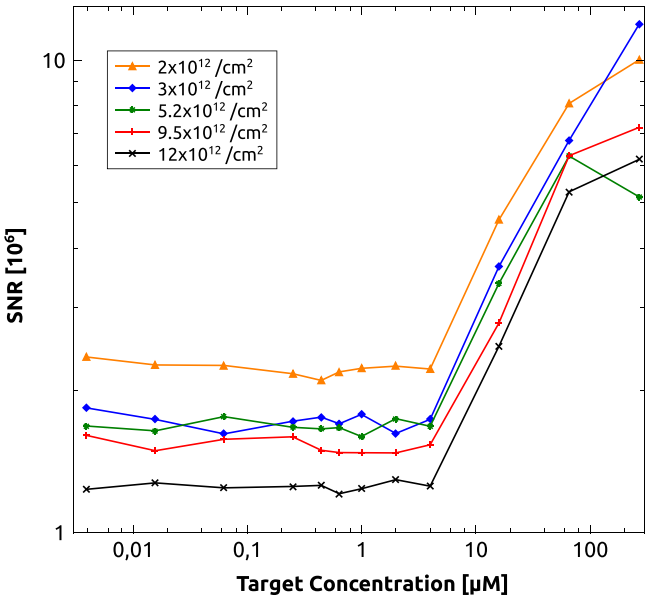

Figure 9. SNR corresponding to figure 8. Its value is constant up to a target concentration of ca. 3 μM.

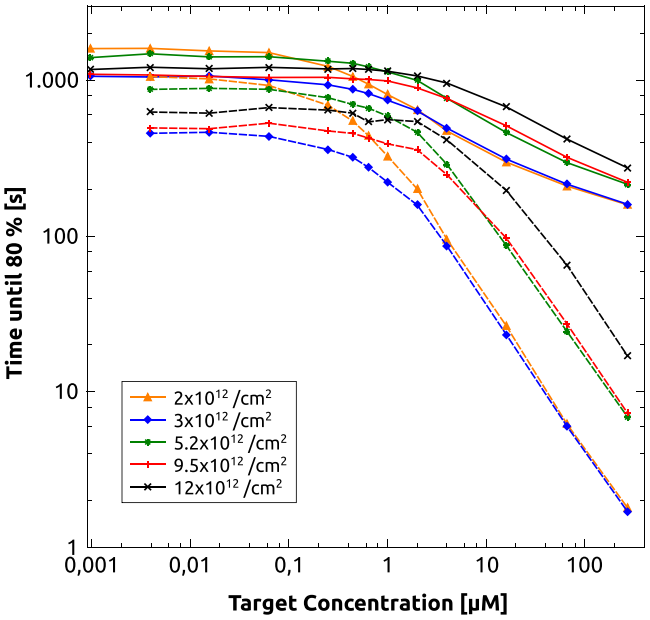

Figure 10. Expected time until 80% of the equilibrium surface-charge density are reached. Solid lines represent solutions where the target molecules are initially in the uppermost simulation box, while the dashed lines represent solutions where a uniform initial concentration is assumed.

is uniform. In the second case, the target molecules enter the liquid from above. As a consequence, the target molecules are initially present only in the uppermost box of the simulation domain. Therefore it takes time until any molecules reach the sensor surface and are detected.

Here we calculate the expected time until 80% of the equilibrium surface-charge density are reached. Of course, this time decreases with increasing target molecule concentration. However, this effect is larger when there is an initially uniform concentration of the target molecules throughout the liquid as shown in figure 10. These simulation results mean that mixing of the liquid is essential for fast detection.

5. Conclusions

We have derived explicit expressions for the expected value, the variance, and the SNR of target molecules at the surface of affinity based sensors for the case where the concentration of target molecules in the liquid is constant. These results answer the question of biological or association–dissociation noise in these sensors. For the more general case of diffusive transport of target molecules, we have implemented and performed stochastic simulations of the coupled reaction-diffusion system to investigate several features of the signal and SNR of nanowire sensors.

The main model system for the biological detection mechanism is hybridization of DNA at a charged surface. We considered various probe densities as well as different target-molecule concentrations. We determined association and dissociation rate constants. They reflect the fact that a higher probe density causes electrostatic-repulsion effects decreasing the binding efficiency. This effect arises in a probe-density range between 3 and 5.2×10^{12} molecules cm^{-2}.

A remarkable feature of such field-effect sensors is that even if the binding efficiency is lower for a certain probe-target concentration pairing, the surface-charge density can be larger and therefore result in better detection by a field-effect sensor. This inversion effect is shown in the simulations results.

In summary, we have discussed the features of the optimal biological detection mechanism within nanowire biosensors and shown how design parameters interrelate and can be optimized.

Acknowledgements

The authors acknowledge support by the FWF (Austrian Science Fund) START project no. Y660 *PDE Models for Nanotechnology*. The authors acknowledge the anonymous referees' comments that helped improve the manuscript. The authors also acknowledge discussions with Alena Bulyha (AIT).

References

[1] Zheng G, Patolsky F, Cui Y, Wang W U and Lieber C M 2005 *Nat. Biotechnol.* **23** 1294–301
[2] Patolsky F, Zheng G and Lieber C M 2006 *Nat. Protocols* **4** 1711–24
[3] Stern E, Klemic J F, Routenberg D A, Wyrembak P N, Turner-Evans D B, Hamilton A D, LaVan D A, Fahmy T M and Reed M A 2007 *Nature* **445** 519–22
[4] Stern E, Vacic A, Rajan N K, Criscione J M, Park J, Ilic B R, Mooney D J, Reed M A and Fahmy T M 2010 *Nat. Nanotechnology* **5** 138–42

[5] Hunt H K and Armani A M 2010 *Nanoscale* **9** 1544–59
[6] Duan X, Li Y, Rajan N K, Routenberg D A, Modis Y and Reed M A 2012 *Nat. Nanotechnology* **7** 401–7
[7] Baumgartner S, Vasicek M and Heitzinger C 2011 *Procedia Eng.* **25** 407–10
[8] Baumgartner S, Vasicek M, Bulyha A and Heitzinger C 2011 *Nanotechnology* **22** 425503 1–8
[9] Baumgartner S and Heitzinger C 2012 *Commun. Math. Sci.* **10** 693–716
[10] Baumgartner S, Vasicek M and Heitzinger C 2012 *Chemical Sensors: Simulation and Modeling: Conductometric-Type Sensors* ed G Korotchenkov vol 2 (New York: Momentum) pp 447–69
[11] Baumgartner S, Heitzinger C, Vacic A and Reed M A 2013 *Nanotechnology* **24** 225503 1–9
[12] Bulyha A and Heitzinger C 2011 *Nanoscale* **3** 1608–17
[13] Tulzer G, Baumgartner S, Brunet E, Mutinati G C, Steinhauer S, Köck A, Barbano P E and Heitzinger C 2013 *Nanotechnology* **24** 315501 1–10
[14] Hassibi A, Navid R, Dutton R W and Lee T H 2004 *J. Appl. Phys.* **96** 1074–82
[15] Hassibi A, Zahedi S, Navid R, Dutton R W and Lee T H 2005 *J. Appl. Phys.* **97** 084701
[16] Hassibi A, Vikalo H and Hajimiri A 2007 *J. Appl. Phys.* **102** 014909
[17] Das S, Vikalo H and Hassibi A 2009 *J. Appl. Phys.* **105** 102021
[18] Deen M J, Shinwari M W, Ranuárez J C and Landheer D 2006 *J. Appl. Phys.* **100** 074703
[19] Peterson A W, Heaton R J and Georgiadis R M 2001 *Nucleic Acids Res.* **29** 5163–68
[20] Gillespie D T 2008 *Formal Methods for Computational Systems Biology* ed M Bernardo, P Degano and G Zavattaro (Berlin: Springer) 125–68
[21] Higham D J 2008 *SIAM Rev.* **50** 347–68
[22] Tirado M M, Martinez C L and de la Torre J G 1984 *J. Chem. Phys.* **81** 2047–52
[23] Tree D R, Muralidhar A, Doyle P S and Dorfman K D 2013 *Macromolecules* **46** 8369–82
[24] Hai-Lang Z and Shi-Jun H 1996 *J. Chem. Eng. Data* **41** 516–20
[25] Erban R, Chapman J and Maini P *Lecture Notes* arXiv: 0704.1908 preprint